AIAA Journal
Vol. 37, No. 10, October 1999

Stability Analysis for Noise-Source Modeling of a Part-Span Flap

Mehdi R. Khorrami* and Bart A. Singer†
High Technology Corporation, Hampton, Virginia 23666

The relevant and important flow features of the local mean flowfield in the vicinity of a flap side edge are extracted from an extensive computational and experimental database. Based on the local flow features, possible mechanisms for flow-induced noise sources that are responsible for sound generation at flap side edges are conjectured. Relatively simple flow models for the dominant noise sources are proposed and developed. The models are based on the most amplified instability modes of the local shear flow. Stability analysis of the modeled flowfield provides an estimate of the frequencies associated with the local flow unsteadiness. Computed frequencies show the proper trend and are in good agreement with NASA Langley Research Center's acoustic microphone array and unsteady surface-pressure measurements.

Nomenclature

c = main chord
f = frequency, Hz
i = $\sqrt{-1}$
M = freestream Mach number
m = parameter adjusting cylindrical shear-layer thickness
N = integrated amplification factor
n = azimuthal wave number
q = vortex swirl parameter
Re = Reynolds number
R_0 = cylindrical shear-layer radius of curvature
r = radial coordinate
r_0 = vortex core radius
U = mean velocity component in x direction
U_0 = constant mean velocity component in x direction
U_∞ = freestream velocity
V = mean velocity component in r direction
W = mean velocity component in θ direction
$W_{\max}$ = maximum tangential velocity in the vortex
x = streamwise coordinate
y = vertical coordinate
y_{rot} = rotated vertical coordinate
z = spanwise coordinate
α = wave number along vortex axis or perpendicular to the plane of the shear layer
β = shear-layer growth rate per radian
δ = parameter defining velocity deficit or excess in the vortex core
δ_f = flap deflection angle
θ = azimuthal coordinate
$\bar{\theta}$ = dummy variable
Φ = perturbed flow variable
ϕ = perturbation complex amplitude function
ω = complex angular frequency
ω_i = imaginary part of angular frequency (growth rate)
$\omega_{i\,\max}$ = maximum growth rate
ω_r = real part of angular frequency
ω_r^* = dimensional real part of angular frequency

Introduction

WITH the design of modern quiet jet engines, the airframe-generated noise of civil transports has become a major concern for noise certification and environmental considerations. Past studies have shown that the high-lift devices, such as slats and flaps, and the landing gears are major contributors to aircraft noise during approach and landing.[1,2] The noise sources at a flap side edge are of primary interest in the present work.

To develop a viable noise prediction and suppression methodology, a good understanding of the mechanism and nature of sound sources at a flap side edge is needed. Unfortunately, the complex flowfield at a flap side edge produces sound sources and sound-generation mechanisms that are poorly understood. The goal of the present research is to further our understanding of the relationship between the noise sources and the predominant local flow features. The effort will spur the development of mean-flow-based semi-analytical design tools that model local flow unsteadiness, which is the driver of the far-field acoustics.

The first attempt at modeling noise radiation from flap side edges was performed by Hardin.[3] In his two-dimensional model, he suggested that boundary-layer turbulence swept from the underside of a flap around the side edge is responsible for the production of noise. To model a turbulent eddy, he considered the convection of concentrated vorticity, embedded in a potential flow, around a sharp edge. Hardin showed that the magnitude of the sound radiation depended on the strength of the convected vorticity field and its distance from the sharp edge. Recently, Sen[4] proposed a new model in terms of a dynamical system in which a stationary point vortex residing at the side edge may be forced to oscillate about its equilibrium position by the incoming turbulence. Hardin and Martin[5] numerically computed the far-field acoustics associated with Sen's model and obtained a relation that relates sound intensity to typical aircraft parameters such as flap chord, thickness, deflection angle, and lift coefficient.

In another model, Howe[6] formulated the side-edge flowfield as a flow through a slot. He obtained an estimate of the surface-pressure fluctuations on the flap top surface just inboard of the side edge and used asymptotic formulas to calculate sound radiation in the limiting cases of very large and very small acoustic wavelengths. In this model, the gap between the side edge of the flap and the undeflected main wing has a strong influence on the intensity of the sound radiation. Although very elegant, this model fails to take into account large flap deflections and the extension of the flap beyond the trailing edge of the undeflected main wing. An overview of various airframe-noise modeling issues in general, and of the flap in particular, is provided by Crighton.[1]

Under NASA's Advanced Subsonic Technology program,[2] a concerted effort toward understanding a flap side-edge flowfield and its acoustic characteristics is underway. The extensive computational and experimental effort is directed at the identification of dominant noise sources in a generic high-lift setting.[7–13] Already a clear picture of the time-averaged, flap-edge local flowfield has emerged from these studies. The present modeling of the noise sources is based on these new insights and the extensive computational and experimental databases that have become available through this

---

Presented as Paper 98-2225 at the AIAA/CEAS 4th Aeroacoustics Conference, Toulouse, France, 2–4 June 1998; received 20 July 1998; revision received 5 February 1999; accepted for publication 9 February 1999. Copyright © 1999 by Mehdi R. Khorrami and Bart A. Singer. Published by the American Institute of Aeronautics and Astronautics, Inc., with permission.

*Senior Scientist, 28 Research Drive. Senior Member AIAA.

†Research Scientist; currently Research Scientist, Aerodynamic and Acoustic Methods Branch, NASA Langley Research Center, Hampton, VA 23681-2199.

program. Because of the complex nature of the problem, our goals have been modest and focused on obtaining an estimate of the frequency range of the unsteadiness supported by the local flow features. We expect that the frequency range of the strongest acoustic signals will overlap the frequency range of the most violent flow unsteadiness. Hence, comparisons of predicted vs measured frequencies will be sufficient to determine whether a particular modeling approach deserves further consideration. Preliminary results of the present work were instrumental in the development of a more elegant and sophisticated model reported by Streett.[14]

The paper is organized as follows. In the next section, an overview of the relevant local flow features is given. Possible noise sources and generation mechanisms are identified and discussed. The modeled flowfields and their stability formulations are presented in the following section. Next, the results of the stability analysis are discussed, and a comparison with the experimentally measured frequencies is made. Finally, we summarize our conclusions.

Local Mean Flowfield

For modeling purposes both experimental and computational databases for a generic two-element configuration provide the flap-edge flowfield in a high-lift setting. This high-lift system, which comprises a main element and a 30% half-span flap, was tested in the NASA Ames Research Center 7 × 10 foot tunnel[7] (hereafter called 7 × 10). The test cases involved an angle of attack of 10 deg and flap deflections of 29 and 39 deg. A smaller (approximately half) scale replica of the model was tested in the NASA Langley Research Center Quiet Flow Facility[8] (QFF) and Basic Aerodynamic Research Tunnel. In the QFF, using a five-hole probe, the side-edge flowfield was mapped thoroughly by Radeztsky et al.[8] The extensive acoustic measurements conducted in the QFF are reported by Meadows et al.[13] The companion computational efforts are discussed in detail by Khorrami et al.,[10] Khorrami et al.,[12] and Takallu and Laflin.[11] The simulations of Khorrami et al.[12] show a remarkable agreement with the experimental measurements of Radeztsky et al.[8] Together, the computations and the experiments provide most of the required information for our modeling effort.

The time-averaged base flow at the flap side edge is shown in the next few figures. Because of other considerations, a left-handed coordinate system is used to present the computed and measured data. Figure 1 displays a view of the flap from underneath. Superimposed on this view is the coordinate system. Length units in this system are normalized with the main chord. The origin is placed at the juncture of the flap leading edge and the side edge. The streamwise coordinate increases toward the flap trailing edge, whereas the spanwise coordinate increases inboard. The normal coordinate increases into the page.

The steady measured and computed flowfield shows the presence of a dual vortex system at the flap edge for both flap deflections. Near the flap leading edge, the boundary layer on the bottom surface separates at the sharp corner and rolls up to form the stronger of the two vortices. This strong vortex resides near the bottom corner (Fig. 2). The adjacent outer flow reattaches on the side edge and forms a thin boundary layer. The newly formed layer separates at the sharp top corner and forms the weaker of the two vortices on the flap top surface (Fig. 3). Because of the constant feeding of vorticity, both vortices gain in strength and size along the flap chord. Downstream of the flap midchord, the side vortex begins to interact and merge with the vortex on the top surface. Eventually a single dominant streamwise vortex is formed (Fig. 4). For the 29-deg flap deflection case, near the trailing edge, the vortex has a jetlike axial velocity reaching twice the freestream velocity. The vortices for the 39-deg flap deflection case are stronger as a result of the higher circulation. Because of the greater adverse pressure gradient in the 39-deg flap deflection case, downstream of the merging location the core of the vortex expands rapidly and vortex breakdown occurs.

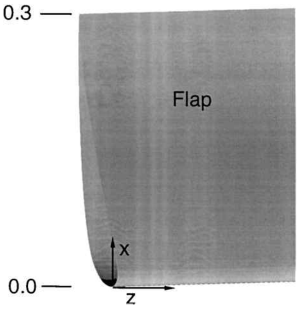

Fig. 1 Bottom view of flap side edge and its coordinate system.

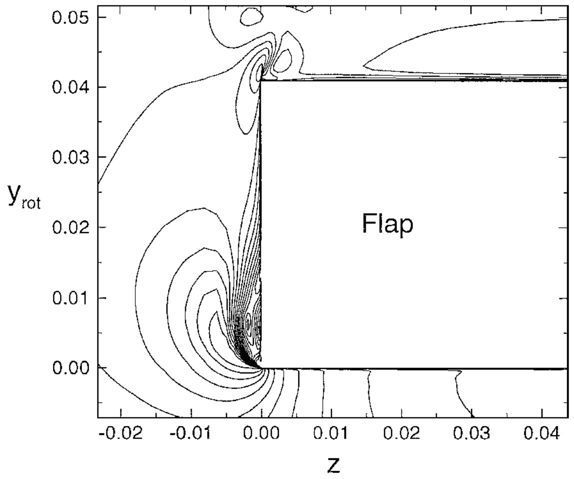

Fig. 2 Spanwise contours of crossflow velocity magnitude near flap leading edge.

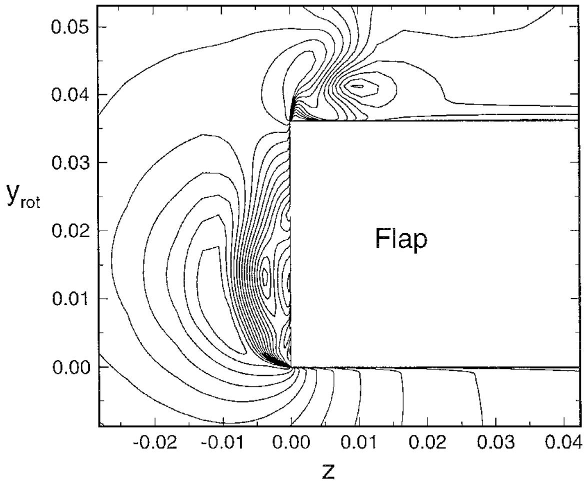

Fig. 3 Spanwise contours of crossflow velocity magnitude upstream of flap midchord.

Acoustic and unsteady surface-pressure measurements, obtained in the QFF experiment, are presented in Ref. 13. A large aperture directional microphone array was used to obtain source localization maps at the side edge. Figure 5 shows the results of Meadows et al.[13] for the 39-deg flap deflection case. For these measurements, the array was located 4 ft (1.22 m) beneath the flap. The numbers indicate the frequency (in kilohertz) associated with the local maximum acoustic signal. Returning to Fig. 5, several distinct trends distinguish themselves. Upstream of the flap midchord, all of the sources are located at the side edge. The higher-frequency sources are situated near the leading edge. The frequency of the sources drops in the downstream direction along the chord. Past the midchord region, the sources gradually move inboard as their frequencies drop further. The scenario is identical for the 29-deg flap deflection except that the sources near the leading edge have lower frequencies and the inboard movement of the source occurs closer to the flap trailing edge. Unfortunately, degradation of signal-to-noise ratio forces us to postpone a detailed discussion of the 29-deg flap case until after the results have been analyzed and fully scrutinized.

Analysis of possible sources of local flow unsteadiness helps in the identification of noise sources. Based on the description of the

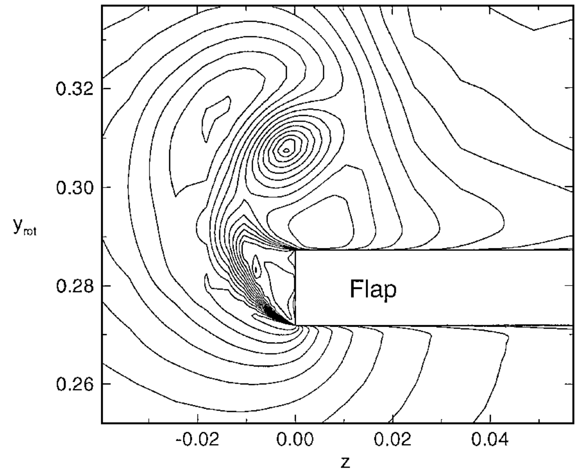

Fig. 4 Spanwise contours of crossflow velocity magnitude downstream of flap midchord.

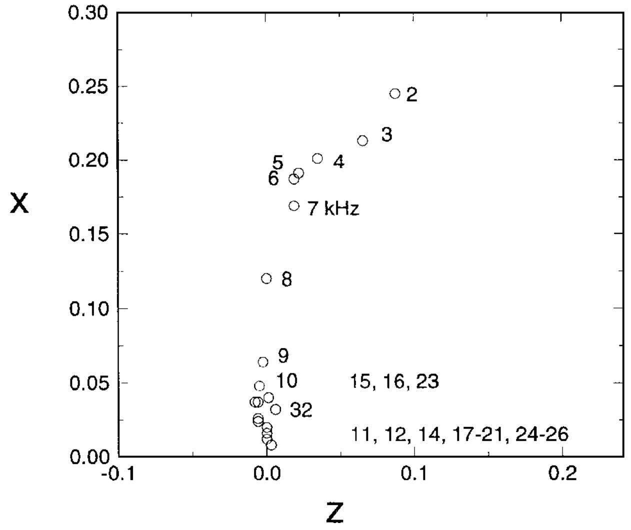

Fig. 5 View from the bottom indicating location of peak amplitude at each frequency at flap side edge for 39-deg deflection. Measurements were obtained in QFF using directional microphone array.

flowfield provided, several flow features lend themselves to being unsteady. They are 1) large-scale flow fluctuations supported by the free-shear layer emanating from the flap bottom edge and spanning the entire flap chord, 2) large-scale flow fluctuations supported by the postmerged vortex downstream of the flap midchord region, 3) convection of a turbulent boundary layer over the sharp edges at the flap side edge, giving rise to scattering and broadband sound radiation, 4) vortex merging, and 5) vortex breakdown.

Of these five likely sources, we believe that the first two are most likely to be responsible for the bulk of the concentrated audible noise generation. Item 3, the problem of turbulent boundary layers past sharp edges (e.g., trailing-edge noise) has received a great deal of attention in the past. Its scaling laws for the far-field sound radiation are well known. The acoustic measurements conducted in the 7 × 10 and QFF do not strictly follow these scalings. Specifically, according to Storms et al.,[15] noise spectral measurements from a small-aperture array in the 7 × 10 experiment suggest a $U^{5.5}$ or higher velocity scaling at high frequencies. Therefore, other important sound sources are likely to be present. Both vortex merging and vortex breakdown are generally fairly low-frequency phenomena and not as important in the audible spectrum as the other items. Although changes in the flowfield induced by both the steady and unsteady components of vortex merging and vortex breakdown are likely to be important in the subsequent development of the flow, these flow phenomena are not believed to be the root cause of the flow unsteadiness that leads to noise radiation. In this paper, we concentrate on the noise generation associated with the first two flow features, namely the amplifying instabilities in the shear layer and the vortex. Although the rapid spatial growth of these disturbances can potentially result in quadrupole-type acoustic radiation, we conjecture that a more efficient mechanism for conversion of hydrodynamic energy to sound is associated with the interaction of these disturbances with geometrical inhomogeneities of the flap edge. The interaction produces the frequency-wavenumber combination that is needed for acoustic radiation.

Flow Model Development

Vortex Model

A schematic of the envisioned noise-generation mechanism supported by the presence of the postmerged vortex is shown in Fig. 6. The vortex resides on the flap top surface near the sharp edge. The question to be answered is whether the vortex supports any form of unsteady fluctuations. Within an appropriate frequency range, these fluctuations can result in strong localized pressure perturbations. In the vicinity of a sharp edge, the unsteady pressure field is a good acoustic radiator, as discussed by Howe.[6]

An efficient method for determining whether local flow structures support unsteadiness is to perturb the steady base flow with time-harmonic oscillations and observe the response of the system. Such a stability analysis requires very smooth mean-flow profiles, smooth enough to incorporate the second derivatives of the velocity field into the stability calculation accurately. Although the computational database provides important information with regard to the vortex strength, tangential and axial velocity profiles, and the vortex core size, the raw simulated data are not smooth enough to be used in instability calculations. Therefore, some sort of modeling is required. Such modeling is actually desired because our eventual goal is to develop semi-empirical noise prediction tools to be incorporated into an aerodynamic design cycle.

To obtain the relevant flow parameters for our vortex model, the computational database for the 29-deg case was postprocessed extensively. We determined that the postmerged single vortex aft of the flap midchord nearly attains an axisymmetric state. The axial velocity is jetlike, achieving values twice the freestream velocity, whereas the tangential velocity is about 0.6–0.7 of the freestream velocity. For this work, the vortex is modeled as a free vortex. Although the proximity of the flap top surface will alter the vortex structure to a certain extent, we believe making the model more complex at this stage is unwarranted because it is unlikely to change the ultimate outcome of the study significantly. A good profile that fits our computed vortex is the similarity solution obtained by Batchelor.[16] His solution was employed successfully to study stability of trailing line vortices.[17]

In cylindrical-polar coordinates (r, θ, x), the three components of the velocity are V, W, and U, respectively. Assuming the base flow is not changing rapidly in the streamwise coordinate x, the similarity solution for such a vortex takes on the form

$$V(r) = 0 \tag{1}$$

$$W(r) = (q/r)\left(1 - e^{-r^2}\right) \tag{2}$$

$$U(r) = 1 + \delta e^{-r^2} \tag{3}$$

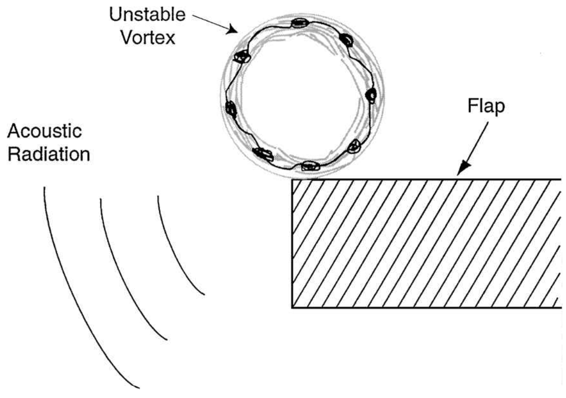

Fig. 6 Envisioned noise-generation mechanism by postmerged vortex.

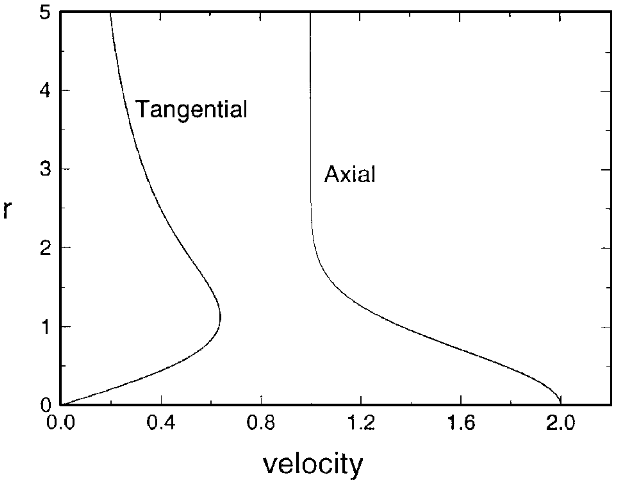

Fig. 7 Velocity profile of modeled vortex.

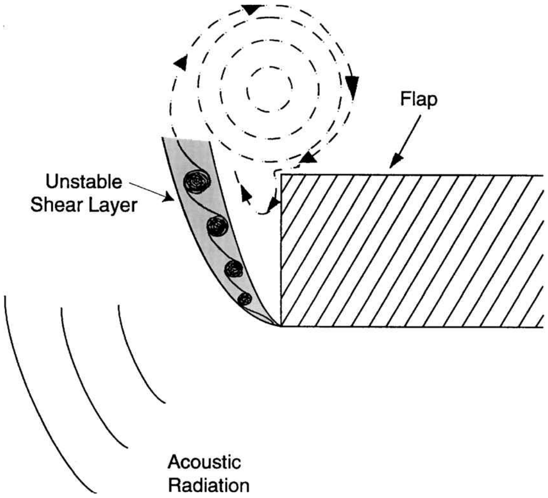

Fig. 8 Envisioned noise-generation mechanism by curved free shear layer.

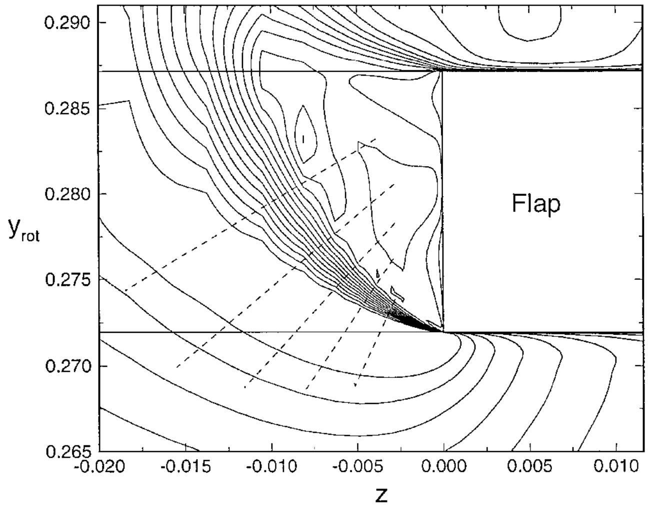

Fig. 9 Typical crossflow velocity magnitude contours at flap side edge showing shear-layer location.

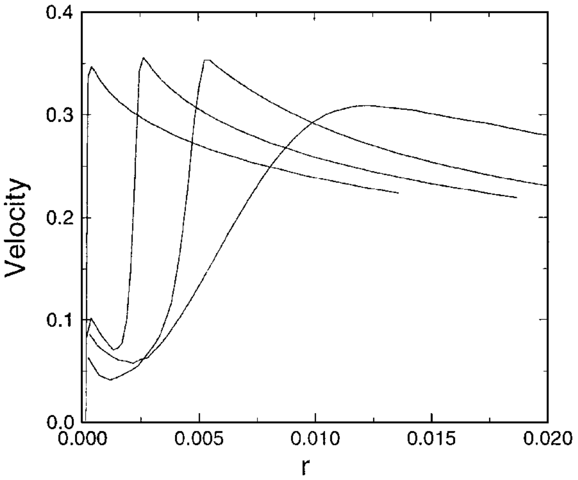

Fig. 10 Computational velocity profiles across shear layer at different angular locations.

In the preceding solution, the normalization has been with respect to U_∞ and r_0. The vortex Reynolds number based on $U_\infty r_0/\nu$ is 5×10^4. To match our computed vortex, both δ and q were set equal to 1.0. Figure 7 shows the variation of axial and tangential velocities with the radial coordinate for our modeled vortex.

Cylindrical Shear-Layer Model

As seen in Figs. 2–4, vorticity is fed to the vortex system at the flap side edge by the separated shear layer at the bottom edge. This shear layer, which has significant curvature, is present along the entire flap chord. A schematic of the local flowfield just aft of the midchord region is shown in Fig. 8. We conjecture that the curved shear layer supports large-scale flow perturbations. After these perturbations are excited, two noise-producing scenarios are possible. In one scenario, the shear-layer fluctuations, which migrate to the outer part of the vortex, are brought to the vicinity of the sharp edges by the vortex velocity field. In the second scenario, these fluctuations move to the vortex interior. If the frequencies of these fluctuations overlap the frequency range of unstable vortex modes, amplifying vortex modes of the type described in the preceding section will be excited. In either case, the unsteady pressure field near the flap sharp edges will radiate sound.

To analyze the possibility of a shear-layer instability, we first model a curved shear layer that resembles the available data. We assume that the fluctuations will be traveling along local flow streamlines. Three-dimensional flow streamlines at the side edge are calculated from the computational data. Both the computational and experimental databases reveal no significant variation in the streamwise velocity across the shear layer. Based on this property of the flowfield, a spanwise planar cut through the computational database is justified. At any desired chordwise location, a spanwise planar cut is made at an angle that contains the local streamlines in the shear layer. A typical cut is shown in Fig. 9, where crossflow velocity contours are plotted.

In Fig. 9, the spatial location, the curved nature, and the thickening of the free-shear layer are apparent. An estimate of the layer's radius of curvature R_0 is obtained for each spanwise slice. Next, the shear layer is cut at several locations normal to its local streamlines (broken lines in Fig. 9) to obtain the crossflow velocity profiles. Several of these profiles are displayed in Fig. 10. Near the bottom edge, the shear layer is very thin. The thin shear layer coincides with a large vorticity concentration and magnitude. The thickness of the layer grows rapidly as the shear layer spreads.

A good model that fits our computed curved shear layer was published by Michalke and Timme[18] in their studies of cylindrical shear layers. The model is a two-parameter family. Normalizing with respect to U_∞ and R_0, in cylindrical-polar coordinates, the model is represented by

$$V(r) = 0 \tag{4}$$

$$W(r) = (q/r)\left(1 - \exp\left\{[-m/(m+1)]r^{2(m+1)}\right\}\right) \tag{5}$$

$$U(r) = U_0 \tag{6}$$

where U_0 without loss of generality can be set to zero. As in Eq. (3), the parameter q sets the magnitude of the maximum velocity, whereas m determines the thickness of the shear layer. The values

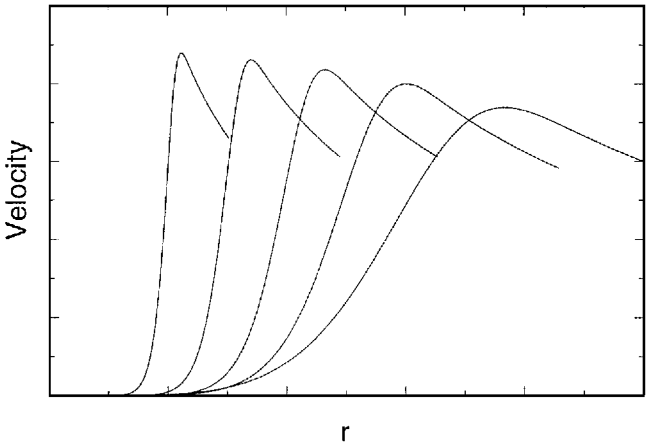

Fig. 11 Velocity profiles of modeled cylindrical shear layer.

for q and m along the shear-layer axis are determined from the local line plots of the type presented in Fig. 10. A sample plot of Eq. (5) is shown in Fig. 11 to illustrate the features of the modeled profile. All of the relevant characteristics of the profiles shown in Fig. 10 are properly captured with this model. In Fig. 11, the values for the velocity and radial coordinate are omitted intentionally because they are scaled to match the local values at each chordwise cutting plane.

Stability Formulation

To obtain the unsteady nature of the local flowfield, we employ linear stability analysis. Although nonlinear effects may play a role at the later stages, we believe linear analysis is the appropriate initial step. The formulation is straightforward, and the results will provide the frequency range of the unsteadiness.

In this formulation, the steady base flow is perturbed with harmonic disturbances and the temporal response of the system is analyzed. The stability analysis assumes viscous incompressible fluids. Although the compressibility effects can be included, the low Mach number of the approach flow suggests that the added complexity will produce results that do not differ appreciably from the incompressible case.

For stability analysis, a normal mode representation of the disturbance field is employed. For our vortex, the perturbations are given as

$$\Phi = \phi(r)\exp[i(\alpha x + n\theta - \omega t)] \tag{7}$$

where Φ can be any one of the primitive variables, such as pressure or any one of the velocity components. In Eq. (7), ϕ is the complex amplitude function, which is dependent on the radial coordinate only. The wave numbers along the vortex axis and tangential directions are α and n, respectively. The complex angular frequency ω is computed as part of the solution. If the sign of the imaginary part of the complex frequency ω_i is positive, the disturbances will grow (unstable), and if it is negative they decay (stable) with time.

For the cylindrical shear-layer model, representation (7) still governs. However, in this case, the x direction is perpendicular to the planar cut and the θ direction is along the curved shear layer.

The procedure to develop the linearized govering equations as well as the equations themselves can be found in the open literature (e.g., Ref. 19) and therefore will not be repeated here. We confine our attention to presenting the results of the stability calculations.

Results and Discussion

Vortex Instabilities

For vortical flows, the source of unsteadiness stems from a combination of the centrifugal instability of the mean flow in conjunction with the presence of mean shear in the axial velocity. Previously, stability analysis for the Batchelor's vortex has shown that this vortex is unstable with respect to both inviscid[17] and viscous[20] instabilities. The inviscid instabilities, however, have significantly larger growth rates than the viscous modes and therefore are of prime interest to us.

To match our computed/measured vortex, the swirl parameter was set to $q = 1.0$, which provided a maximum tangential velocity $W_{\max} \approx 0.64$. A value of 1.0 was assigned to the jet parameter δ, which produced a centerline axial velocity twice the freestream velocity. As mentioned in the preceding sections, the flow Reynolds number was set at 5×10^4.

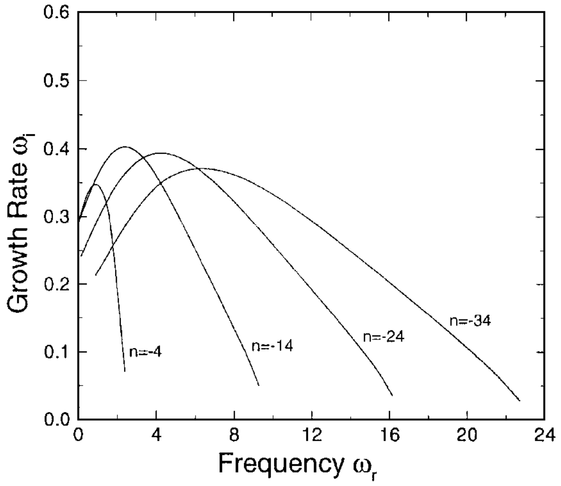

Fig. 12 Vortex instability modes.

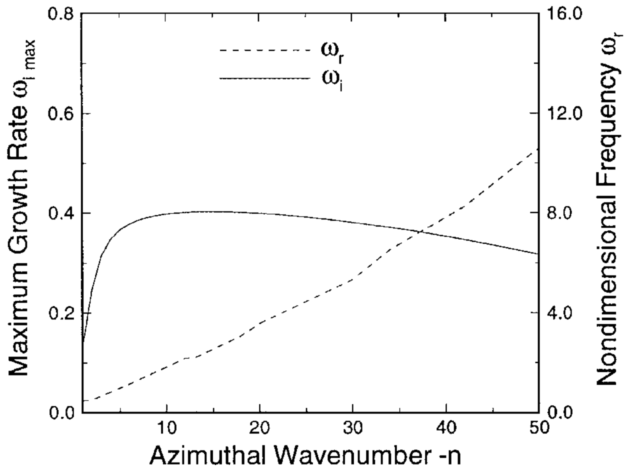

Fig. 13 Maximum growth rates and corresponding frequencies for vortex instability modes.

Stability results for our modeled vortex are shown in Fig. 12. The plots show variation of the growth rate with frequency for several azimuthal wave numbers. For a jetlike axial velocity, the inviscid vortex instabilities are confined to the region in parameter space where the azimuthal wave number is negative. For helical disturbances, the sign of n represents the orientation of the wave (left-hand or right-hand screw), whereas the sign of ω_r/n determines the direction of the propagating wave in the $r-\theta$ plane. In Fig. 12, several trends are worth observing. First, the growth rates associated with these disturbances are quite large. This suggests that the vortex is a good amplifier of flow oscillations, and depending on the initial amplitude, significant levels of flow unsteadiness are reached very rapidly. Second, the vortex is unstable with respect to a broad band of azimuthal wave numbers starting with $n = -1$ (not shown). For our flow conditions, the maximum possible amplification occurs for $-18 \le n \le -12$. Third, the frequency space where flow unsteadiness is permissible is quite large. To show the last two trends more clearly, we have plotted the maximum growth rates and the associated frequencies for each individual n in Fig. 13.

We have performed computations up to $n = -50$. Initially, the maximum growth-rate curve rises very rapidly, but beyond $n = -5$ the curve becomes and stays relatively flat for a wide band of azimuthal wave numbers. The gradual drop in the $\omega_{i\,\max}$ for $n < -15$ is the result of viscous effects. The rate of viscous damping becomes increasingly large for higher azimuthal wave numbers until, depending on the value of Reynolds number, it stabilizes the high-frequency disturbances. To convert from angular to dimensional frequency, we need an estimate for the relevant length scale r_0. From our computational and experimental database, the vortex core radius was found to be approximately 1.0 and 0.5 cm based on 7 × 10 and QFF scaling, respectively. From Fig. 13 we have

$$0.5 < \frac{\omega_r^* r_0}{U_\infty} < 10.5 \tag{8}$$

Using the U_∞ for an $M = 0.2$ flow, the respective frequency ranges for the 7 × 10 and QFF experiments are approximately

$$560\,\mathrm{Hz} < f < 11.7\,\mathrm{kHz} \tag{9}$$

for 7 × 10

$$1.1\,\mathrm{kHz} < f < 23.4\,\mathrm{kHz} \tag{10}$$

for QFF.

The upper frequency of the range is the frequency associated with the $n = -50$ maximum growth rate and thus must be viewed as a somewhat subjective frequency limit. Had we extended the computations beyond this wave number, higher frequencies would have emerged. A more relevant frequency range is obtained from consideration of peak amplification rates. In this flow, the peak amplification rates occur for

$$2 < \frac{\omega_r^* r_0}{U_\infty} < 4 \tag{11}$$

which correspond approximately to

$$2.25\,\mathrm{kHz} < f < 4.5\,\mathrm{kHz} \tag{12}$$

for 7 × 10

$$4.5\,\mathrm{kHz} < f < 9\,\mathrm{kHz} \tag{13}$$

for QFF. However, the peak is quite broad and other frequencies, if present in the flow, will amplify.

Meadows et al.[13] presented extensive unsteady surface pressure measurements at the flap side edge in the QFF experiment. Their coherence results show the presence of a strong source of unsteadiness in the $0 < f < 10\,\mathrm{kHz}$ range for both 29- and 39-deg flap deflections. The strongest correlation occurs between the sensors that reside in the flap midchord and aft of the midchord sections on the top surface near the side edge. The computed flowfield of Khorrami et al.[12] suggests that these transducers lie under the side-edge vortex trajectory. The estimated frequency range for the most amplified disturbances [Eq. (13)] does show the proper range and is also in good agreement with the source localization map (Fig. 5) aft of the flap midchord region. We believe the drop in the frequency as the source moves inboard (Fig. 5) is caused by the rapid growth of the vortex core radius resulting from the flap adverse pressure gradient. The frequency of the most amplified disturbances drops as the vortex core expands. In the present analysis, we have assumed changes along the vortex axis to be negligible and the flow to be parallel. In this regard, the analysis fails to account for the effect of core expansion and the shift in the frequencies. Nevertheless, we think the estimated frequency range for the local flow unsteadiness quite satisfactory.

Cylindrical Shear-Layer Instabilities

For the shear layer, the instability mechanism is of the inflectional type and therefore inviscid in nature. Preliminary results indicated a very weak dependence of growth rates on the Reynolds number when greater than 3×10^3. All of the results that we present were performed for $Re \geq 8 \times 10^3$. For the cylindrical shear layer, Michalke and Timme[18] reported that two-dimensional disturbances ($\alpha = 0$) are the most amplified; three-dimensional perturbations have smaller growth rates. Therefore, in this study, only two-dimensional flow oscillations are considered. Moreover, Fig. 4 shows that the shear layer spans a distance not much more than a quarter of a circle. The lower values of n that have wavelengths greater than the circumferential extent of the shear layer are excluded from our studies. In addition, Fig. 4 illustrates that the thickness of the shear layer increases significantly as it traverses the side edge. Unlike the vortex case, for the cylindrical shear layer, we must account for the effect of increased shear-layer thickness on the amplification of the local flow unsteadiness.

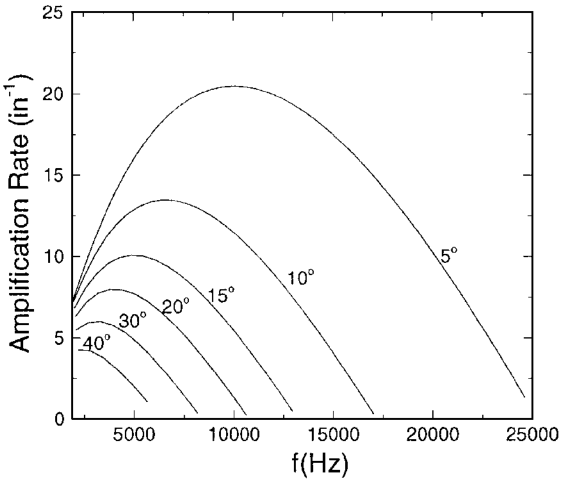

Fig. 14 Typical frequency response curves of cylindrical shear layer. Dimensionalization corresponds to the 7 × 10 experiment.

The effect of the thickening shear layer is at least partially modeled by our use of local velocity profiles at each station along the shear layer. Figure 14 shows local amplification rates as a function of frequency for various circumferential locations along the cylindrical shear layer. The angles refer to angular displacements from the bottom corner of the flap side edge. The data have been dimensionalized to correspond to the 7 × 10 experiments. As the disturbances travel along the shear layer (increasing angle), the shear layer thickens and the amplification rates decrease. The high frequencies, which are very strongly amplified at small angular displacements, become stable, and the frequency of maximum local amplification shifts to lower frequencies.

Rather than simply comparing local amplification, we estimated the total growth of the various disturbances by integrating the local growth rates, much as an N-factor calculation is used in determining transition location.[21] At each circumferential position, the stability calculation assumes that the local flow is parallel. However, the thickening of the shear layer is implicitly considered when the growth rates at the different circumferential locations are integrated to obtain the N factor. For the cylindrical shear layer, the N factor is defined as

$$N = \int_0^{\theta} \beta \,\mathrm{d}\bar{\theta} \tag{14}$$

where θ is the angle over which the disturbance has grown and $\beta = n\omega_i/\omega_r$ is the growth rate per radian around the arc. The stability calculations provide the values of ω_i and ω_r for various n at the different circumferential locations indicated by the dashed lines in Fig. 9. Because the frequency is not known a priori but is computed as part of the solution to the eigenvalue problem, interpolation must be used to obtain growth rates at constant frequency. The resultant values of β at each frequency are integrated. In our case, straightforward trapezoid rule integration is used.

The frequency at which maximum growth (maximum N factor) occurs varies along the shear layer. If we assume that the radiated noise is proportional to the magnitude of the flow unsteadiness, then the frequency of maximum disturbance amplification corresponds to the frequency of the maximum acoustic levels. Figure 15 shows a map of the frequency of the maximally amplified disturbance as a function of chordwise position on the flap. Results for both 29- and 39-deg flap deflections are shown. These data are superposed on the map of frequencies of maximum acoustic radiation as measured by the QFF acoustic array and shown earlier as Fig. 5.

The numbers to the left of $z = 0.0$ correspond to frequencies associated with the maximum N factor at the various locations. In a region extending from the flap leading edge to a location slightly past its midchord (a region where we believe the cylindrical shear layer is the dominant noise source), the instability mechanism is consistent

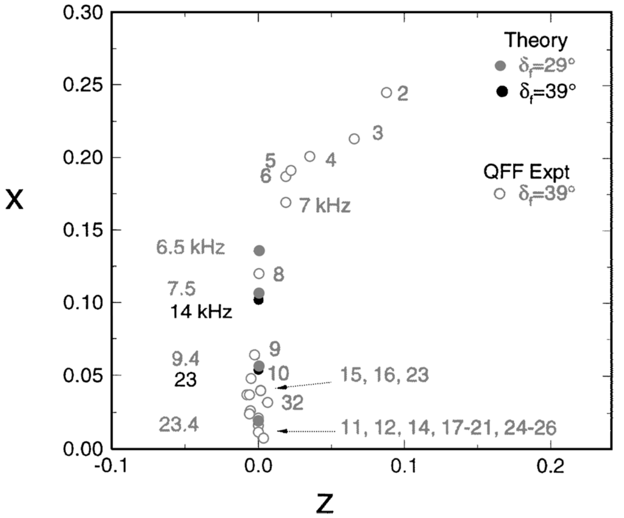

Fig. 15 Frequency of maximally amplified disturbance as function of chordwise position on flap, superposed on QFF acoustic array source map.

with two important experimentally observed trends. That is, the stability results correctly show the trends of decreasing source frequency with downstream distance and increasing source frequency with higher flap deflections. This general agreement of the theoretical predictions with the experimental results suggests that additional work investigating instability mechanisms is warranted.

Conclusion

Environmental noise considerations demand the development of novel noise-reduction techniques and the integration of acoustic and aerodynamic design cycles for future civil transport vehicles. Such an approach requires incorporation of flow physics into any predictive acoustic tools rather than reliance on straightforward empiricism. The present work is a first step toward the development of physics-based models for flap side-edge flowfields.

A detailed picture of the local mean flow at a generic flap edge is constructed from an extensive computational and experimental database. The main features of the side-edge flowfield are a dual-vortex system and a curved shear layer. We conjectured that both of these flow features support flow unsteadiness and thus provide a mechanism for noise generation. Two relatively simple models are developed to model the vortex and the curved shear layer. Both models capture the pertinent features of the respective field.

With linear stability analysis used, the modeled local fields are shown to be good amplifiers of flow unsteadiness. The frequency range of permissible flow unsteadiness is quite broad and is consistent with the frequency ranges observed in measured acoustic signals. For the cylindrical shear-layer instability, the frequencies of the maximally amplified disturbances at various streamwise locations are in good agreement with the directional microphone array measurements performed in the QFF at NASA Langley Research Center.

Acknowledgments

This work was done under NASA Contract NAS1-20059. The authors would like to thank Meelan Choudhari and Craig Streett for stimulating discussions related to the instability mechanisms and Michele Macaraeg for facilitating continued support for this work.

References

[1] Crighton, D., "Airframe Noise," *Aeroacoustics of Flight Vehicles: Theory and Practice*, NASA Reference Publication 1258, Vol. 1, edited by H. H. Hubbard, WRDC TR 90-3052, Aug. 1991.

[2] Macaraeg, M. G., "Fundamental Investigations of Airframe Noise," AIAA Paper 98-2224, June 1998.

[3] Hardin, J. C., "Noise Radiation from the Side Edges of Flaps," *AIAA Journal*, Vol. 18, No. 5, 1980, pp. 549–552.

[4] Sen, R., "Local Dynamics and Acoustics in a Simple 2D Model of Airfoil Lateral-Edge Noise," AIAA Paper 96-1673, May 1996.

[5] Hardin, J. C., and Martin, J. E., "Flap Side-Edge Noise: Acoustic Analysis of Sen's Model," *AIAA Journal*, Vol. 35, No. 5, 1997, pp. 810–815.

[6] Howe, M. S., "On the Generation of Side-Edge Flap Noise," *Journal of Sound and Vibration*, Vol. 80, No. 4, 1982, pp. 555–573.

[7] Storms, B. L., Takahashi, T. T., and Ross, J. C., "Aerodynamic Influence of a Finite-Span Flap on a Simple Wing," Society of Automotive Engineers, SAE Paper 951977, Los Angeles, Sept. 1995.

[8] Radeztsky, R. H., Singer, B. A., and Khorrami, M. R., "Detailed Measurements of a Flap Side-Edge Flow Field," AIAA Paper 98-0700, Jan. 1998.

[9] Mathias, D. L., Roth, K. R., Ross, J. C., Rogers, S. E., and Cummings, R. M., "Navier–Stokes Analysis of the Flow About a Flap Edge," AIAA Paper 95-0185, Jan. 1995.

[10] Khorrami, M. R., Singer, B. A., and Takallu, M. A., "Analysis of Flap Side-Edge Flow Field for Identification and Modeling of Possible Noise Sources," Society of Automotive Engineers, SAE Paper 971917, Traverse City, MI, May 1997.

[11] Takallu, M. A., and Laflin, K. R., "Reynolds-Averaged Navier–Stokes Simulations of Two Partial-Span Flap Wing Experiments," AIAA Paper 98-0701, Jan. 1998.

[12] Khorrami, M. R., Singer, B. A., and Radeztsky, R. H., Jr., "Reynolds-Averaged Navier–Stokes Computations of a Flap-Side-Edge Flowfield," *AIAA Journal*, Vol. 37, No. 1, 1999, pp. 14–22.

[13] Meadows, K. R., Brooks, T. F., Humphreys, W. M., Hunter, W. H., and Gerhold, C. H., "Aeroacoustic Measurements of a Wing-Flap Configuration," AIAA Paper 97-1595, May 1997.

[14] Streett, C. L., "Numerical Simulation of Fluctuations Leading to Noise in a Flap-Edge Flowfield," AIAA Paper 98-0628, Jan. 1998.

[15] Storms, B. L., Ross, J. C., Horne, W. C., Hayes, J. A., Dougherty, R. P., Underbrink, J. R., Scharpf, D. F., and Moriarty, P. J., "An Aeroacoustic Study of an Unswept Wing with a Three-Dimensional High-Lift System," NASA TM-1998-112222, Feb. 1998.

[16] Batchelor, G. K., "Axial Flow in the Trailing Line Vortices," *Journal of Fluid Mechanics*, Vol. 20, 1964, pp. 645–658.

[17] Lessen, M., Singh, P. J., and Paillet, F., "The Stability of a Trailing Line Vortex. Part 1. Inviscid Theory," *Journal of Fluid Mechanics*, Vol. 63, 1974, pp. 753–763.

[18] Michalke, A., and Timme, A., "On the Inviscid Instability of Certain Two-Dimensional Vortex-Type Flows," *Journal of Fluid Mechanics*, Vol. 29, 1967, pp. 647–666.

[19] Khorrami, M. R., Malik, M. R., and Ash, R. L., "Application of Spectral Collocation Techniques to the Stability of Swirling Flows," *Journal of Computational Physics*, Vol. 81, No. 1, 1989, pp. 206–229.

[20] Khorrami, M. R., "On the Viscous Modes of Instability of a Trailing Line Vortex," *Journal of Fluid Mechanics*, Vol. 225, 1991, pp. 197–212.

[21] Bushnell, D. M., and Malik, M. R., "Application of Stability Theory to Laminar Flow Control—Progress and Requirements," *Proceedings: Symposium on the Stability of Time Dependent and Spatially Varying Flows*, edited by D. L. Dwoyer and M. Y. Hussaini, Springer–Verlag, New York, 1987, pp. 1–17.

P. J. Morris
Associate Editor